Acta Oceanol. Sin., 2022, Vol. 41, No. 4, P. 1–13
https://doi.org/10.1007/s13131-021/1847-6
http://www.aosocean.com
E-mail: ocean2@hyxb.org.cn

Submesoscale motions and their seasonality in the northern Bay of Bengal

Lanman Li[1], Xuhua Cheng[1, 2*], Zhiyou Jing[3], Haijin Cao[1], Tao Feng[1, 2]

[1] College of Oceanography, Hohai University, Nanjing 210098, China

[2] Southern Marine Science and Engineering Guangdong Laboratory (Zhuhai), Zhuhai 519080, China

[3] State Key Laboratory of Tropical Oceanography, South China Sea Institute of Oceanology, Chinese Academy of Sciences, Guangzhou 510301, China

Received 9 February 2021; accepted 29 May 2021

Abstract

The unbalanced submesoscale motions and their seasonality in the northern Bay of Bengal (BoB) are investigated using outputs of the high resolution regional oceanic modeling system. Submesoscale motions in the forms of filaments and eddies are present in the upper mixed layer during the whole annual cycle. Submesoscale motions show an obvious seasonality, in which they are active during the winter and spring but weak during the summer and fall. Their seasonality is associated with the mixed layer instability that depends on the mixed layer depth (MLD). During the winter, the MLD provides a much greater reservoir of the available potential energy, which promotes mixed layer instability to develop active submesoscale motions. The variations of MLD are likely modulated by the larger scale motions and the influxes of freshwater. Further investigations imply that the MLD and the stratified barrier layer are combined to determine the vertical structure of the submesoscale motions. The shallow MLD and strong stratification below during the summer and fall seem to prevent the downward extension of submesoscale motions. But in spring when the weak stratification exists, the penetration depth exceeds the base of the barrier layer.

Key words: submesoscale motions, seasonality, northern BoB, mixed layer instability, stratification

Citation: Li Lanman, Cheng Xuhua, Jing Zhiyou, Cao Haijin, Feng Tao. 2022. Submesoscale motions and their seasonality in the northern Bay of Bengal. Acta Oceanologica Sinica, 41(4): 1–13, doi: 10.1007/s13131-021/1847-6

1 Introduction

The Bay of Bengal (BoB) is a semiclosed bay of the northeastern Indian Ocean, where the hydrologic and dynamic characteristics are remarkably different from those of other regions. The BoB is forced by the semiannual reversal monsoon that is southwest from June to September and northeast from November to January (Schott et al., 2009). The basin is dominated by a strong cyclonic circulation during the northeast monsoon and by an anticyclonic circulation during the southwest monsoon (Eigenheer and Quadfasel, 2000; Somayajulu et al., 2003; Qiu et al., 2007). The enormous amount of precipitation caused by the strong and wet southwesterly wind, combined with runoff discharged mainly by the Ganges-Brahmaputra and the Irrawaddy River, directly discharge abundant freshwater into the bay during the summer and fall. This creates shallow freshwater pools and strong salinity stratification near the surface (Behara and Vinayachandran, 2016; Rahaman et al., 2014). Stratification usually leads to the defining vertical structure of this region: a shallow mixed layer, thick barrier layer (BL), and temperature inversion layer (TIL) (Dandapat et al., 2020; Han et al., 2001; Howden and Murtugudde, 2001; Thadathil et al., 2016). TIL that is fully formed during the winter (Thadathil et al., 2016) maintains the warm surface temperature by vertical mixing (Sengupta et al., 2008; Thadathil et al., 2016). BL starts to develop during the fall and is thickest during the winter (Ma et al., 2020; Thadathil et al., 2007; Qiu et al., 2012). Strong stratification prevents the exchange of cool interior water and warm upper water, consequently maintaining warm surface temperatures that intensify the tropical cyclones (Balaguru et al., 2012; Neetu et al., 2012).

The northern BoB features abundant multiscale dynamical processes. The results from the satellite observations and numerical models reveal that mesoscale eddies are rich in the northern bay, and their features and variability have been substantially studied (Babu et al., 1991; Chen et al., 2012; Cheng et al., 2013, 2018). The northern coast of the BoB is influenced by the coastally trapped Kelvin waves that propagate from the equator (Vialard et al., 2009; Cheng et al., 2013; Suresh et al., 2013). Tides in the area are ample, with amplitudes typically greater than 2 m, and display the most variable seasonality in the global ocean with typical amplitudes ranging from 10 cm to 20 cm (Tazkia et al., 2017). The interaction between tides and topography easily produces internal waves that are often observed during nonmonsoons (Jithin et al., 2020; Phaniharam et al., 2020). As the spatial resolution of satellite observations increases, submesoscale motions in this region are noted. Based on high-resolution (~5 km) observations from the moderate-resolution imaging spectroradiometer (MODIS), the sea surface temperature reveals that fine temperature filaments and fronts at typical scales of O (10) km are ubiquitous in the northern bay (Fig. 1) and are richer during the winter (Fig. 1b).

Foundation item: The National Key R&D Program of China under contract No. 2018YFA0605702; the National Natural Science Foundation of China under contract Nos 41876002 and 41776002.
*Corresponding author, E-mail: xuhuacheng@hhu.edu.cn

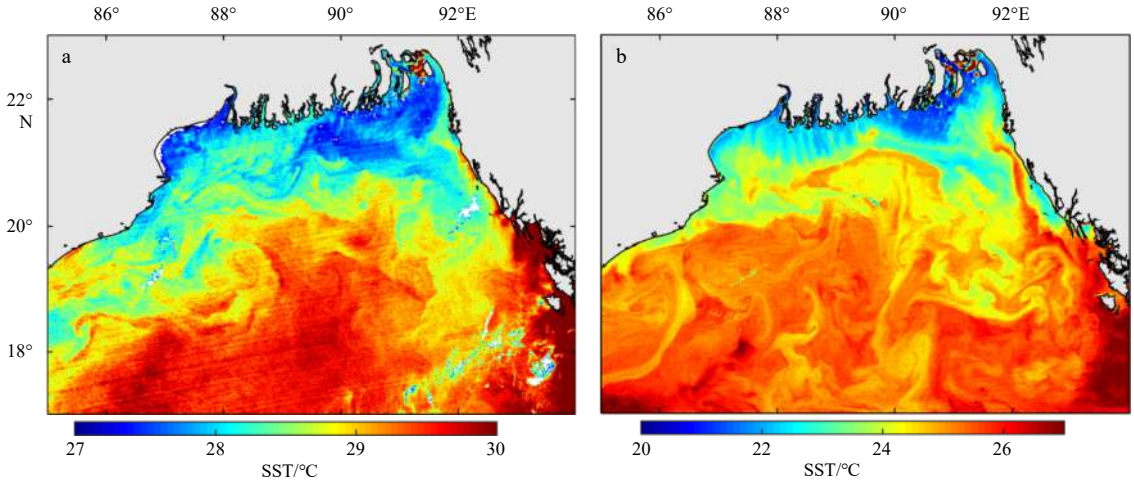

Fig. 1. Sea surface temperature (SST) on November 11, 2020 (a), and January 30, 2018 (b) from moderate-resolution imaging spectrora-diometer.

Submesoscale processes with a horizontal scale of *O* (1–10) km and a temporal scale of *O* (1) day provide a conduit for the energy cascade between multiscale (Capet et al., 2008d; McWilliam, 2016; Molemaker et al., 2010). Their strong vertical motions are vital for the upper ocean heat budget and biogeochemical characteristics (Klein and Lapeyre, 2009; Mahadevan, 2016; Su et al., 2018). In the open upper ocean, frontogenesis and mixed layer instability are considered as the dominant generation mechanisms for submesoscale processes (Callies et al., 2015; Mcwilliams, 2016; Thomas et al., 2008).

The seasonality of submesoscale motions exhibits geographical dependency (Lin et al., 2020; Zhang et al., 2020; Dong and Zhong, 2018; Dong et al., 2020; Brannigan et al., 2015; Mensa et al., 2013; Wang et al., 2018) associated with distinct background dynamical features. Based on observations, previous studies have revealed that salinity-controlled fronts with lateral scales of *O* (1–10) km are ubiquitous in the upper northern BoB (Ramachandran et al., 2018; Sengupta et al., 2016). Strong submesoscale fronts in this region are associated with frontal instabilities, subsequently effecting the vertical and horizontal variability of properties, such as stratification, potential vorticity, temperature, and salinity (Pham and Sarkar, 2019; Ramachandran and Tandon, 2020; Sarkar et al., 2016). The submesoscale dynamics in the Indian Ocean has received much fewer attentions compared with other oceans. Strong horizontal density gradient and stratification in the northern BoB provide a favorable condition for the occurrence of submesoscale processes. Due to the lack of observations and model simulations, it is still a great challenge to systematically investigate the submesoscale processes in the BoB.

This study provides a basic description of the seasonal features of submesoscale motions in the northern BoB and their corresponding mechanisms based on the regional oceanic model system (ROMS) with high spatial resolution. Under the presence of stratification, their effect on the characteristics of submesoscale motions is interesting. This article is constructed as follows: Section 2 describes the configuration of ROMS; Section 3 presents the seasonal variations in submesoscale motions; Section 4 discusses the potential mechanisms that are probably responsible for the seasonality; Section 5 explores the relationship between stratification and submesoscale motions; Conclusions and discussion follow in Section 6.

2 Data and methods

2.1 *Data*

2.1.1 *Observation data*

The vertical temperature and salinity data provided by the daily Research Moored Array for African-Asian-Australian Monsoon Analysis and Prediction (RAMA) buoy and the gridded monthly reconstructed Argo products are compared with the ROMS simulation in Section 5.1. The RAMA buoy located at 15°N, 90°E for a period from January 2009 to February 2010 is chosen. The Argo products range from 2002 to 2015, with a spatial resolution of 0.5°×0.5°. Vertically, the temperature and salinity for two datasets are available at discrete depth intervals. They have been interpolated by 1 m interval above 100 m.

2.1.2 *Model setup*

The model that was applied to explore submesoscale motions in this study was ROMS (Shchepetkin and McWilliams, 2005). To capture the submesoscale motions, ROMS used one-way nesting to increase the resolution from parent grid simulation. The parent zone covers the North Indian Ocean and the northwestern Pacific Ocean (Fig. 2a) with a lower horizontal resolution (LR) of ~7.5 km, while the child zone covers the BoB (Fig. 2b) with a higher resolution (HR) of ~1.5 km. The vertical resolution is 60 levels, which includes 25 layers at the upper 200 m. The vertical mixing scheme for momentum and tracers is based on the K-profile parameterization (Large et al., 1994). The bathymetry is derived from the GEBCO_08 (General Bathymetric Chart of the Oceans) dataset.

The parent simulation was forced by the daily mean climatology wind stress from the Quick Scatterometer (QuikSCAT). The heat and freshwater fluxes were provided by the monthly climatology of the International Comprehensive Ocean-Atmosphere Data Set (ICOADS) (Woodruff et al., 2011). The initial and lateral boundary conditions were provided by the monthly averaged climatology of Simple Ocean Data Assimilation (SODA) reanalysis dataset (Carton and Giese, 2008). The parent configuration was spun up for 20 years, then run for an additional 14 months to provide the boundary condition for child simulation. Then both simulations were performed for 14 months and saved every 3 days from January 2 to February 29 of the next year. Both simu-

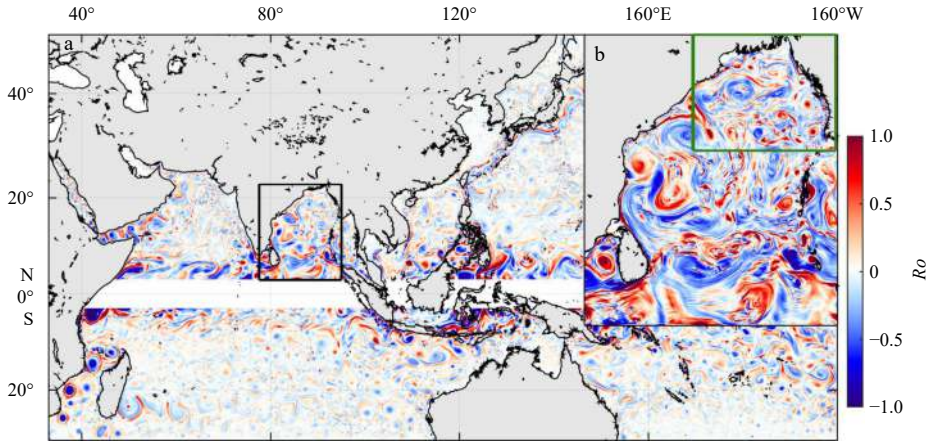

Fig. 2. Spatial distribution of the Rossby number (*Ro*) at 5 m depth from the lower resolution (a) and higher resolution (b) simulation. The location of the study region is denoted by the green box on b.

lated outputs are corresponding to the climatological field rather than the realistic period. This method adopting the climatological forcing has been successfully applied in the simulating submesoscale motions (Gula et al., 2014; Jing et al., 2021; Cao et al., 2021).

Submesoscale motions are highly correlated with the salinity fronts in this region. The monthly-averaged salinity at 5 m depth is compared between ROMS HR (whole year) and Argo (2002–2015) in Figs 3a and b, respectively. Both results show that low salinity water rapidly develops during the summer monsoon. Generally, the monthly evolution of salinity in ROMS is in agreement with the Argo results, illustrating the ability of the model simulation. Note that the simulated salinity is fresher than the Argo result, which may be caused by the differences between initial salinity in the model and Argo salinity. Since we focused on the seasonal variations, this salinity difference has less impact on the result of our study.

2.2 *Methods*

2.2.1 *Flow decomposition*

Ocean flows contain multiscale processes that can disturb the analysis of the submesoscale variations. For convenience, the flow field is divided into two parts: large-mesoscale $\bar{U}$ and submesoscale U'. A Reynolds decomposition is employed in this study. The submesoscale component U' is obtained by high-pass filtering in spatial domain, with a spectral cutoff on the Fourier transform spectrum to obtain an approximate Reynolds average. The remaining velocity is defined as $\bar{U}$. The partition scales are selected as 15 km based on the scale of the disturbance under the baroclinic instability $L = NH/f$, where N denotes the buoyancy frequency, f is the Coriolis parameter, and H denotes the mixed layer depth (MLD). The MLD is computed by the depth at which the density is larger than the surface of 0.2 kg/m^3 (Narvekar and Kumar, 2006).

To examine whether 15 km is the typical decomposition scale, a spectral method that counts the ratio of the contributions of divergent and rotational to kinetic energy is used (Torres et al., 2018). When the ratio is close to 0.1, the contribution of the divergent part is not negligible, implying the role of submesoscale motions. The spectral method is provided in supplementary materials. The estimated scale is 16 km, which is close to 15 km. As the minimum scale of the model resolving is 5 times of the horizontal resolution (Lévy et al., 2012), the submesoscale can be resolved in the high-resolution child configuration.

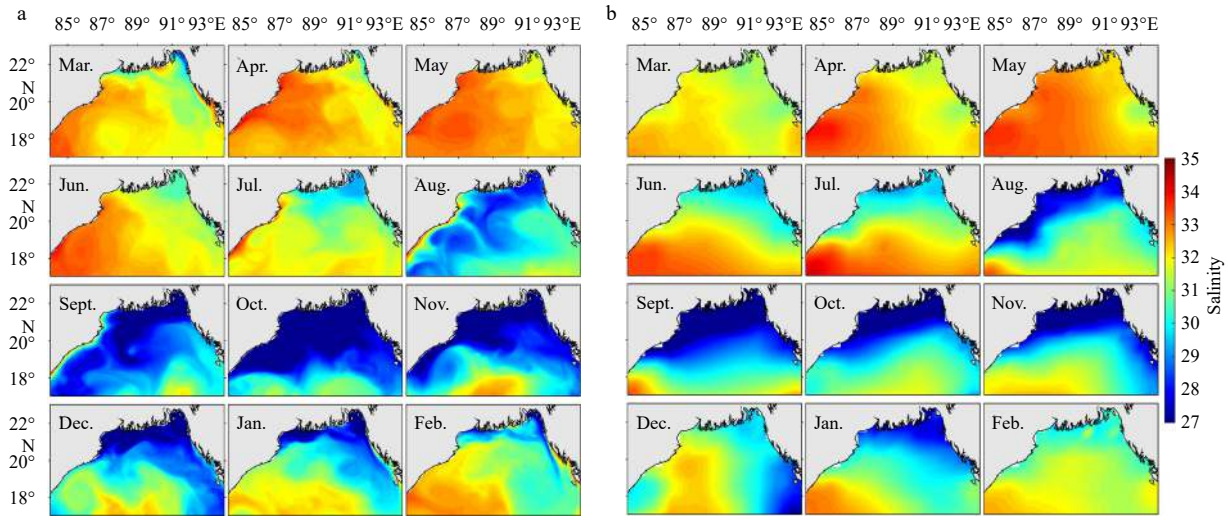

Fig. 3. Monthly mean salinity at 5 m depth from regional oceanic modeling system higher resolution (a) and the monthly climatological Argo product (b).

2.2.2 *Definition of the vertical structure and stratification*

The layer between the mixed layer and isothermal layer is BL (Vinayachandran et al., 2002). The barrier layer thickness (BLT) is defined as the depth difference between the MLD and the isothermal layer depth (ILD), where BLT=ILD–MLD. The ILD is the depth at which the temperature decreases by 0.6°C from the surface (Ma et al., 2020). In this study, the TIL is defined at which the temperature is warmer than that at the surface by 0.1°C (Girishkumar et al., 2013). The BL usually exists simultaneously with the TIL during winter in the northern BoB. Both the BL and TIL are sandwiched between the surface layer and subsurface colder layer.

The density in the mixed layer is relatively uniform. The isothermal layer, as the definition implies, is a layer with uniform temperature. When vertical salinity stratification is absent and the density distribution is entirely controlled by the temperature, the thermocline layer and the mixed layer coincide. Once the halocline shoal to a depth smaller than the thermocline, a BL forms. The BL and TIL are usually associated with high stratification. The squared buoyancy frequency $N^2 = -g\partial\rho/\partial z$, indicating the density stratification, is contributed by two components: salinity $N_S^2 = -g\beta\partial S/\partial z$ and temperature $N_T^2 = g\alpha\partial T/\partial z$, where ρ is the density, g is the gravity acceleration, S is the salinity, T is the temperature, β is the haline contraction coefficient and α is the thermal expansion coefficient (Maes, 2008).

3 Main characteristics of submesoscale motions

3.1 *Horizontal distribution of submesoscale motions*

Submesoscale motions are characterized by $O(1)$ Rossby number ($Ro = \zeta/f$), which means their relative vorticity ($\zeta = v_x - u_y$) is roughly equivalent to the planetary vorticity f (Thomas et al., 2008). Snapshots of the *Ro* in four seasons in both HR and LR are shown in Fig. 4. The large *Ro* features that manifest as filaments and eddies are conspicuous in the maps for different times, indicating that submesoscales are widespread in the northern BoB. Compared with HR (Figs 4a, b), submesoscale motions are greatly underestimated in LR (Figs 4e, f), and the mesoscale processes occupy the domain. Complex patterns with high *Ro* occur in most of the time except in January (Fig. 4a). High *Ro* are conspicuous in the region where the water depth is deeper than 50 m (called the offshore region in the following descrip-

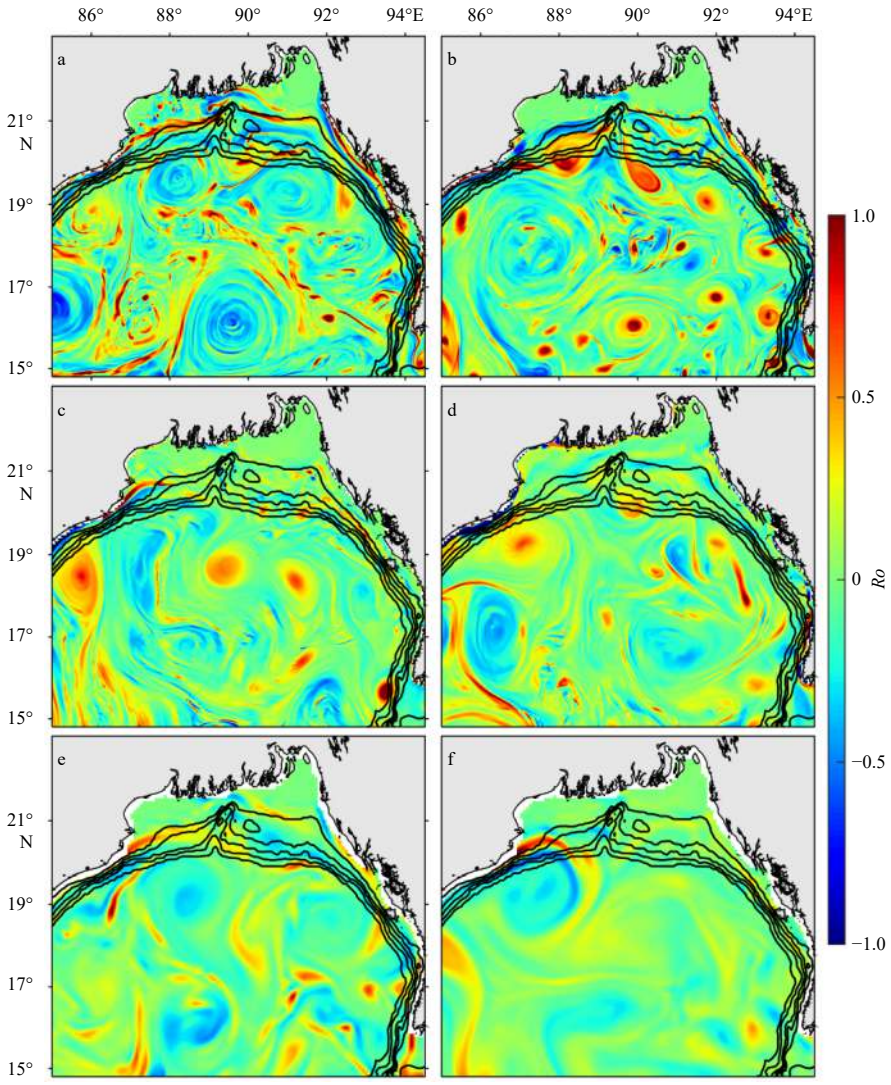

Fig. 4. Spatial distribution of Rossby number (*Ro*) from regional oceanic modeling system higher resolution simulation on January 23 (a), March 23 (b), June 20 (c), and October 23 (d) and from lower resolution regional oceanic modeling system simulation on January 23 (e) and June 20 (f). The black isobaths show the depth at 50 m, 100 m, 200 m, 500 m, 1 000 m, respectively.

tion). The time series of *Ro* averaged over the whole region (gray line) and the offshore region (blue line) are shown in Fig. 5a. A good correspondence between the two series is noted with a correlation coefficient of 0.97, and their difference is small. The following analyses mainly focus on the offshore region.

Snapshots of *Ro* suggest that submesoscale motions have a significant variability throughout the year (Figs 4a–d). Submesoscale features are most active during the winter, mainly in the forms of filaments and eddies (Fig. 4a). Then, they gradually weaken from spring to fall. Compared to the winter monsoon (winter and spring), submesoscale motions are relatively quiescent during the summer monsoon (summer and fall). In the northern bay, a clear seasonal cycle of *Ro* is observed, with a peak in January and a trough in August, indirectly reflecting the variability of submesoscale motions.

3.2 *Vertical structure of submesoscale motions*

The typical features of submesoscale motions are the high *Ro* and the strong vertical velocity (w). The temporal and vertical distribution characteristics of the regionally-averaged *Ro* and w are shown in Fig. 5. High values of *Ro* occur at the upper mixed layer and can penetrate under the MLD. The mean value of $|Ro|$ is 0.17 at the surface and only 0.07 at 200 m depth (Fig. 5a). The time series of regionally-averaged MLD has a good correspondence with ζ and w, indicating that the variability of submesoscale motions is probably related to the mixed layer processes (Figs 5b, c). The vertical structures of *Ro* and w also show obvious seasonal variations (Figs 5b, c). Strong vertical exchanges induced by submesoscale motions are the most active at approximately 25 m during the winter monsoon (Fig. 5c), especially in the winter. For the boundary condition that near surface $w \approx 0$, the seasonality of w in the upper 10 m is insignificant. It should be noted that the LR simulation mostly indicates the mesoscale processes (not shown), which tend to have similar seasonality with submesoscale processes, seemingly suggesting that the submesoscale processes are closely related to the local mesoscale processes. The annual cycle of submesoscale motions in this region is distinguished from that in the northern Gulf of Mexico, where a secondary maximum for submesoscale motions emerges during summer (Luo et al., 2016) and is similar to the Gulf Stream region (Callies et al., 2015) and the Kuroshio Current region (Mensa et al., 2013; Qiu et al., 2014). It is noted that the mean $|w|$ is still strong below 100 m from June to February, which is probably induced by the interaction between the current and topography in the northern boundary (Molemaker et al., 2015).

Skewness (S_k) in the distribution of normalized relative vorticity (*Ro*) is one of the features of submesoscale flows (Buckingham et al., 2016). The probability density function (PDF) and skewness of *Ro* is one metric for analyzing submesoscale motions. The PDF distributions of *Ro* at 5 m for both simulations for four seasons are represented in Fig. 6. In HR, the positive vorticity overwhelms negative vorticity for all seasons, indicated by positive skewness. The prevailing positive vorticity has been noted by previous studies (Capet et al., 2008b; Lin et al., 2020; Qiu et al., 2014) and interpreted as being due to submesoscale instability (centrifugal instability). When a large anticyclonic vorticity is present ($\zeta < -f$), centrifugal instability arises and suppresses the growth of large negative vorticity motion but has no effect on positive vorticity motion. The probability of positive vorticity in HR continuously decrease from spring to fall, while negative vorticity with the maximum values during the fall (Fig. 6a). The skewness has a maximum of 1.29 in spring, then decreases in winter, and reaches a much lower value in the summer and fall. The extraordinarily large negative vorticity is probably related to submesoscale processes that are induced by the interaction between the southwestward flow and topography. For LR, the maximum positive vorticity is approximately a second of those in HR, showing a rapid decrease in vorticity in the mesoscale resolving simulation. The corresponding skewness is low in LR (Fig. 6b), and the PDF of vorticity becomes more symmetric.

4 Interpretation of the seasonality of submesoscale motions

The above results show that submesoscale motions are mostly present during the winter and spring, and in the upper layer. The potential generating mechanisms are investigated in this section.

4.1 *Frontogenesis*

In the upper layer, frontogenesis is an important mechanism for the generation of submesoscale fronts. Frontogenesis is that larger-scale strain intensifies the cross-front density gradients (Hoskins and Bretherton, 1972). Here, strain is defined as $S_t = \sqrt{(\partial u/\partial x - \partial v/\partial y)^2 + (\partial u/\partial x + \partial v/\partial x)^2}$, where u and v are zonal and meridional velocity, respectively. The strain consists of along-front stretching and the cross-front shear (Mahadevan and Tandon, 2006). As horizontal density gradient is enhanced, the vertical secondary circulation is produced, which suppresses the sharpen of the front and tends to restore the geostrophic balance by tilting isopycnals toward horizontal (Capet et al., 2008c). The evolution rate of the front induced by the strain can be depicted by the frontogenesis rate F, $F = \frac{\mathrm{D}|\nabla_h \rho|^2}{\mathrm{D}t} = -\left(u_x \rho_x + v_x \rho_y\right) \rho_x - \left(u_y \rho_x + v_y \rho_y\right) \rho_y$, where $|\nabla_h \rho|^2$ denotes the intensity of the front (Capet et al., 2008c; Hoskins, 1982; Hoskins

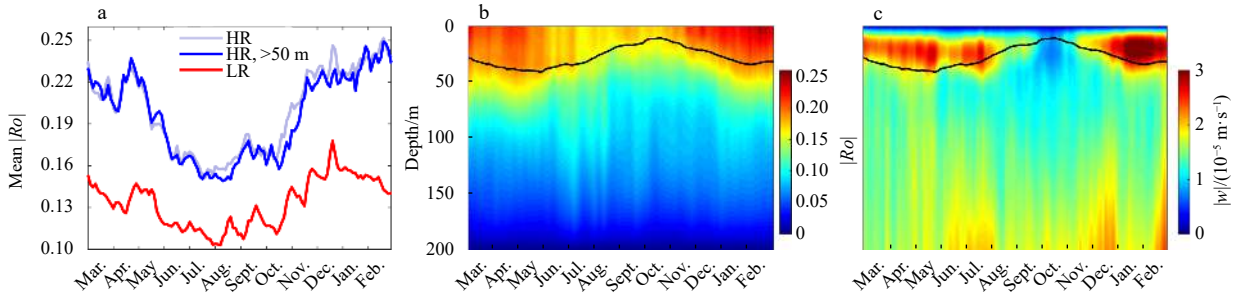

Fig. 5. Time series of the regionally-mean $|Ro|$ at 5 m depth averaged over the whole northern region from higher resolution (HR) (gray line) and lower resolution (LR) (red line) simulation, and over the region where the water column is deeper than 50 m from HR (blue line) simulation (a). The vertical profiles of regionally-averaged $|Ro|$ (b), and $|w|$ (c) in HR as a function of time. The black curve denotes the mixed layer depth.

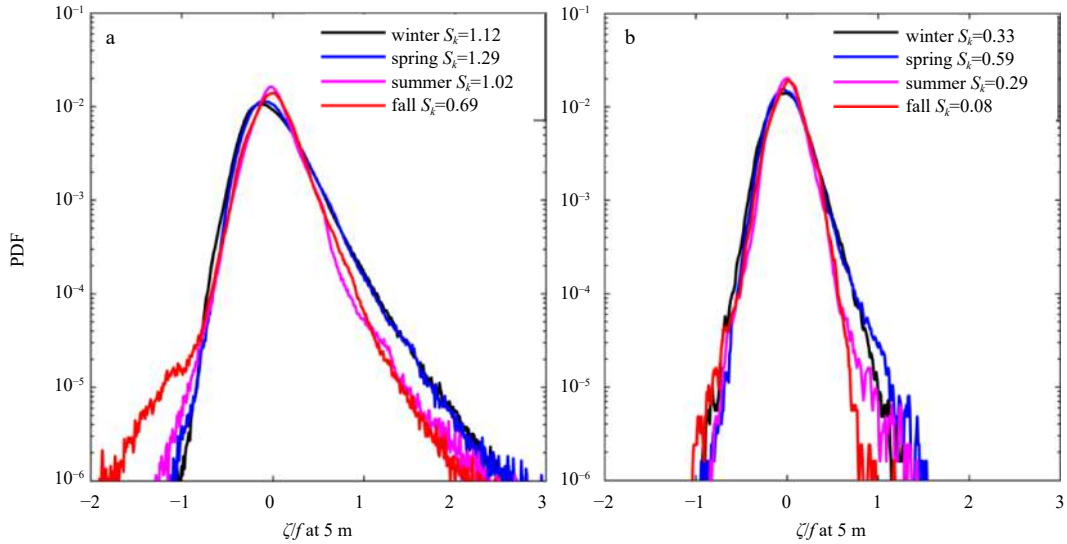

Fig. 6. Probability density function (PDF) of *Ro* at 5 m depth over the offshore region from higher resolution (a) and lower resolution simulation (b). The black, blue, magenta, and red lines denote the results in winter (December–February), spring (March–May), summer (June–August), fall (September–November), respectively.

and Bretherton, 1972). Above, u and v denote the zonal and meridional velocity, ρ is the density, and the subscript is the derivative. Strong strain rates and active horizontal density gradients are conducive to the generation of submesoscale motions (Dong and Zhong, 2018; Gula et al., 2014; McWilliams, 2016).

Figure 7a shows the F varied with time and depth. As the resolution becomes finer, the regionally-averaged magnitude of F increases (Figs 7a, b). Positive F almost appears in the upper mixed layer, implying that frontogenesis mainly occurs in the upper ocean, similar to findings of other studies (Brannigan et al.,

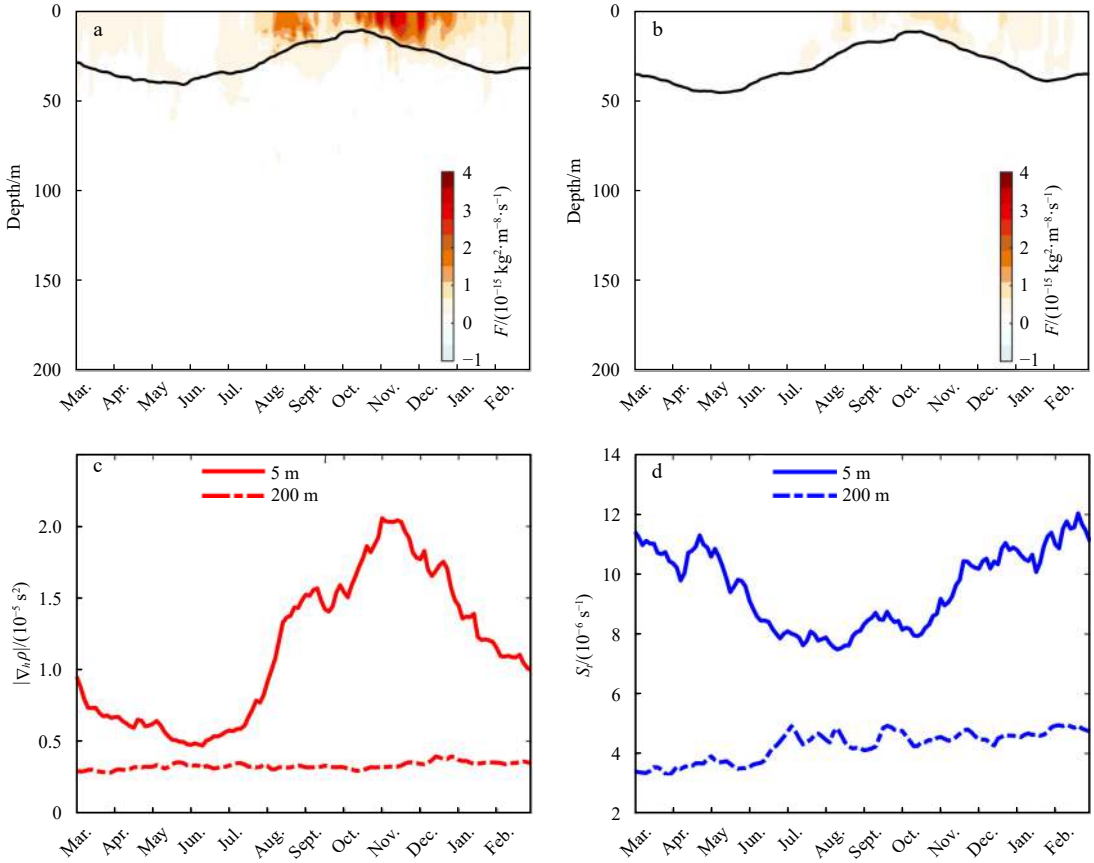

Fig. 7. Vertical and temporal evolutions of the regionally-averaged frontogenesis F in higher resolution (a), and b is the same as a, but in lower resolution simulation. The black line denotes the mixed layer depth. The time series of horizontal density gradient $|\nabla_h\rho|$ (c), and strain S_t (d) at 5 m depth (solid line) and at 200 m depth (dashed line).

2015; McWilliams, 2017). High values for F are trapped in the shallow mixed layer during the late summer and fall. For the period with the deep mixed layer (spring and winter), F is in a weak state. The magnitude of frontogenesis in the late summer and fall is an order of magnitude higher than the rest of the time is novel.

The time series of $|\nabla_h\rho|$ and S_t at different depths are shown in Figs 7c and d, respectively. Both S_t and $|\nabla_h\rho|$ are stronger at the 5 m depth where high Ro frequently appears. The temporal variations in F show a good correlation with horizontal density gradients (r=0.82), and is insignificantly correlated with the strain rate (r=–0.26). These results indicate that density gradients are the dominant factors for frontogenesis and that the strain rate has a relatively weak influence. The increasing horizontal density gradients in summer and fall, which may be created by the influxes of freshwater (Shetye, 1993), feed the evolution of frontogenesis and lead to the much higher F (Luo et al., 2016). The correlation between F and $|Ro|$ averaged with the MLD is only –0.39. Frontogenesis seems not to be the controlling factor for the submesoscale motions during the whole year. However, frontogenesis is likely to play an important role during summer and fall.

4.2 *Mixed layer instabilities*

The mixed layer is not entirely homogeneous but has numerous horizontal density gradients overlying the strongly stratified layer (Boccaletti et al., 2007). Baroclinic instability that occurs in the mixed layer is called MLIs and can be measured by the conversion rate of available potential energy (APE) to submesoscale eddy kinetic energy (EKE), that is PK. The PK is defined as the vertical buoyancy flux ($w'b'$) averaged over the mixed layer, which is calculated as $\mathrm{PK}=\dfrac{\int_0^{-\mathrm{MLD}} w'b'\mathrm{d}z}{\mathrm{MLD}}$ (Boccaletti et al., 2007), where w is the vertical velocity, b is the buoyancy ($b=-g\rho/\rho_0$, g is the gravitational acceleration, ρ_0 is the reference density defined as the density averaged over the region and the mixed layer), and the prime indicates the submesoscale component. The scaling of $w'b'$ in the upper boundary layer appears to follow a relationship $\mathrm{PK}=\langle w'b'\rangle_{xyz}\propto\langle|\nabla\bar{b}|\rangle^2_{xyz}\cdot\langle\mathrm{MLD}\rangle^2_{xy}$ (Fox-Kemper and Ferrari, 2008; Fox-Kemper et al., 2008; Capet et al., 2008a), where $\langle\ \rangle_{xyz}$ indicates the volume averaged over the domain and MLD. Conceptually, the scaling assumes that horizontal buoyancy gradients and MLD are two main factors influencing MLIs.

As shown in Fig. 8a, PK is always positive, implying the transition from APE to EKE. The high value of PK is mainly concentrated in the mixed layer and becomes small beneath the mixed layer (not shown). It is reasonable to infer that MLIs occur mainly in the mixed layer. Within the mixed layer, PK gradually decreases from the spring to fall, then sharply increases in the late fall, reaching a maximum in winter. The correlation coefficient between the variations of PK and Ro is 0.68. PK in spring are much smaller than that in winter, while submesoscales are as strong as winter. The larger PK in winter is possible related to the scale of the fronts in the background (Fig. S2). The larger scale fronts prevail in spring and turn smaller fronts in winter. These strong fronts combined with deep mixed layer contribute to the generation of submesoscale. The small-scale fronts in winter significantly enhance the b', resulting in a larger PK. There may be other mechanisms for the occurrence of submesoscale processes in spring, which need further exploration with a comprehensive model.

PK scaling has been verified successfully by Capet et al. (2008a) in the Argentinian shelf and by Mensa et al. (2013) in the Gulf Stream. To test the parameterization scheme, $\langle|\nabla\bar{b}|\rangle^2_{xyz}\cdot\langle\mathrm{MLD}\rangle^2_{xy}$ is shown by the red line in Fig. 8a. Overall, the scaling is appropriate in this region. The time series of $\langle|\nabla\bar{b}|\rangle^2_{xyz}$ and $\langle\mathrm{MLD}\rangle^2_{xy}$ are plotted in Fig. 8b. MLD obviously displays an opposite seasonality with respect to horizontal density gradients. MLD is deep in the winter and spring, consistent with the strong submesoscale motions. A significant enhancement of buoyancy gradients can be observed during the summer and fall, which does not have a significant influence on the formation of MLIs. The results illustrate that the MLD is potentially the main controlling factor in submesoscale motions formation.

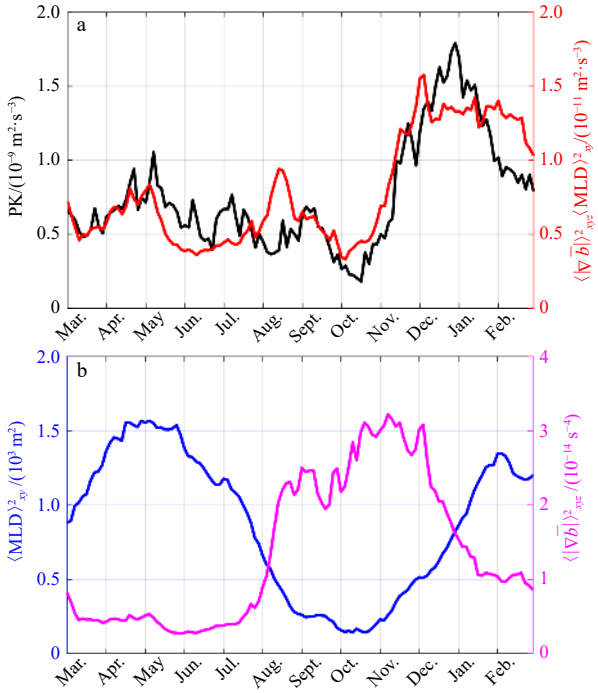

Fig. 8. Time series of the PK (black) and $\langle|\nabla\bar{b}|\rangle^2_{xyz}\cdot\langle\mathrm{MLD}\rangle^2_{xy}$ (red) (a), and time series of the $\langle|\nabla\bar{b}|\rangle^2_{xyz}$ (magenta) and $\langle\mathrm{MLD}\rangle^2_{xy}$ (blue) at 5 m depth (b).

The seasonal variations in MLD can be partially linked to vertical stratification in the ocean. The vertical sections of density and salinity along 19°N in spring, winter, and fall are shown in Fig. 9. In spring and winter, the outcropping isopycnals accompany deep MLD, which provide a favorable condition to store APE that feeds the development of submesoscale motions (Figs 9a, b). In contrast, the MLD is shallowest in fall, when the stratification is the strongest and the upper thin mixed layer is isolated from the interior (Fig. 9c). Strong stratification is likely to limit the generation of submesoscale motions by inhibiting the formation of vertical recirculation along the fronts.

When the averaged surface salinity is compared with the MLD and horizontal buoyancy gradients, we find that these three-time series are better correlated, with correlation coefficients reaching 0.96 and –0.91, respectively (Fig. 10a). The salinity gradually decreases from June to October. As reported by Akhil et al. (2014), the freshest water appears in the northern BoB especially during and post the summer monsoon. The seasonal cycle of salinity is highly correlated with the influxes of the runoff and precipitation, which further produce strong salinity stratification and a shallow MLD (Narvekar and Kumar, 2006; Vinayachandran et al., 2002; Rao and Sivakumar, 2003). After the injection of freshwater encounters salty seawater, enormous salinity

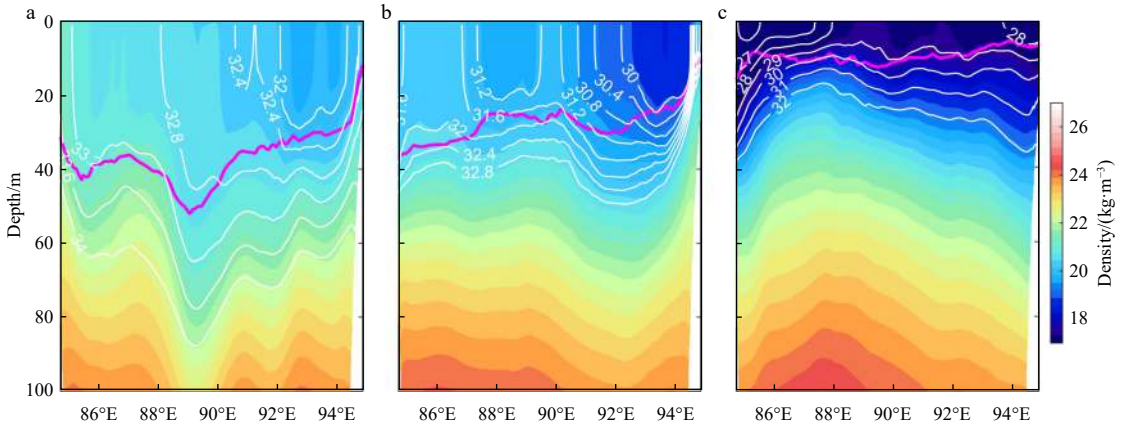

Fig. 9. Vertical section of density (color) and salinity (white contours) along the 19°N in spring (a), winter (b) and fall (c). The magenta lines indicate the mixed layer depth.

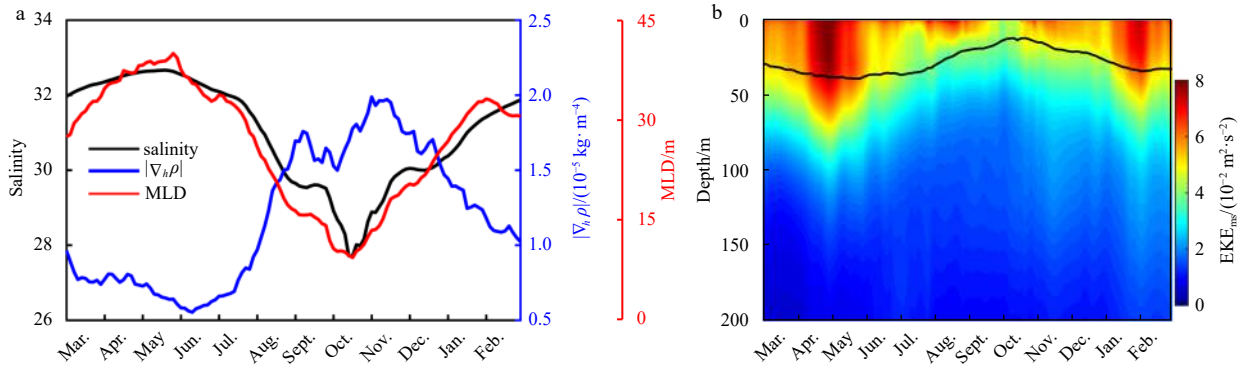

Fig. 10. The annual cycle of regionally-mean salinity (black line), horizontal density gradients $|\nabla_h\rho|$ (blue line), and mixed layer depth (MLD) (red line) at 5 m from higher resolution simulation (a), and the seasonal variations in the regionally-mean eddy kinetic energy (EKE) of mesoscale processes as a function of depth (b). The black line in b is the MLD.

fronts (high buoyancy gradients) are formed. The influxes of freshwater in this region are a critical factor influencing the variations in MLD and buoyancy gradients, especially in the summer and fall. In addition, the vertical and annual cycles of the eddy kinetic energy (EKE $= 1/2(\bar{u}^2 + \bar{v}^2)$) are shown in Fig. 10b. Active mesoscale processes may be another factor supporting the submesoscale motions generated during the winter monsoon, and probably indirectly through modulating the deepening of the mixed layer. The periphery of mesoscale eddy is usually accompanying the active submesoscale motions (Yang et al., 2017).

5 Relationship between stratification and submesoscale motions

The above descriptions imply that MLD is an important factor for the spatial distribution of submesoscale motions. The deeper the MLD is, the submesoscale motions can penetrate deeper. Previous studies suggested that thick BL and a TIL exist in the northern BoB in winter (Ma et al., 2020; Thadathil et al., 2007, 2016), which tends to shrink the thickness of the MLD. BL and TIL are a highly stratified layers. Their possible influence on submesoscale motions in the northern BoB has been less studied.

5.1 *The BL and TIL in the model*

Time-depth sections of temperature, salinity, MLD, ILD, and TIL in the northern BoB from the model and observations are displayed in Fig. 11. The BL exists persistently for the whole year but obviously thickens during the fall and then fully develops during the winter. The reproduced BL in ROMS is basically in concert with the observations. Notably, the annual cycle ILD in ROMS is weaker than the observations. The probable reasons may be the climatological daily atmospheric forcing used in the model. During the fall and winter, temperature inversion is evident, which weakens the stratification in the upper ocean and potentially has impacts on the submesoscale motions.

The annual means of BLT and TIL are shown in Fig. 12, and they display a spatial difference. The thickest BL and TIL occur in the northern bay and gradually weaken to the central bay. Their thickness in the northern bay is approximately 3 times larger than that in the central bay. The submesoscale processes in two sub-regions, the northern region (NR) and the central region (CR), are further analyzed in the next section. The distribution of the annual mean BL in the model is consistent with that in Thadathil et al. (2007). The freshwater from runoff and precipitation in the upper layer significantly influence the forming of BL and TIL (Vinayachandran et al., 2002; Thadathil et al., 2016). They create a thin freshwater surface layer and a more strongly stratified interior below, which are favorable for the development of BLT and TIL. As far away from the coast, the inflow of runoff decreases, their effect on the formation of BLT and TIL weaken.

5.2 *Potential impact of BL and TIL on the submesoscale motions*

The temporal-vertical evolution of *Ro* and w in NR and CR are shown in Fig. 13, superimposed with the MLD, ILD, and TIL. Al-

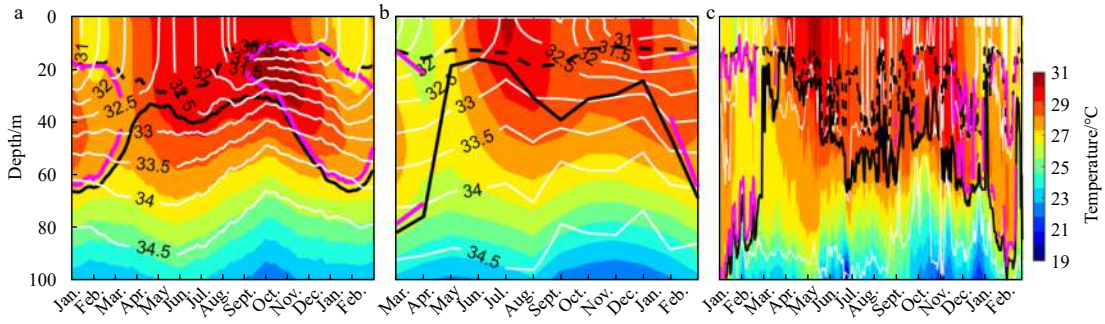

Fig. 11. Time-depth variations in the temperature (color) and salinity (white contours) in the regional oceanic modeling system higher resolution (a), Argo products (climatology) (b), and RAMA buoys (c) (January 2009 to February 2010). The regionally-averaged mixed layer depth (MLD), isothermal layer depth (ILD), and temperature inversion layer (TIL) are presented by the black dashed, black solid lines, and magenta lines, respectively.

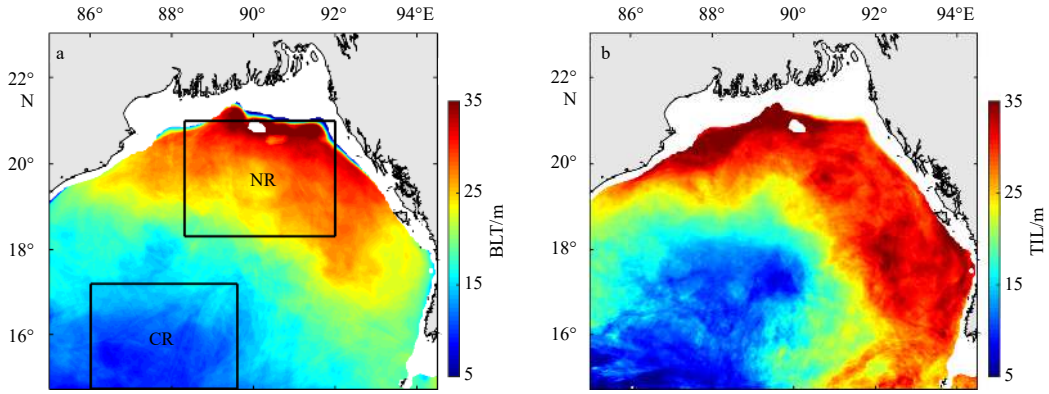

Fig. 12. Spatial distribution of annual mean barrier layer thickness (BLT) (a) and temperature inversion layer (TIL) (b) in higher resolution. The offshore regions are colorless. The two black boxes indicate the northern region (NR) and central region (CR), which are further analyzed in Figs 13 and 14.

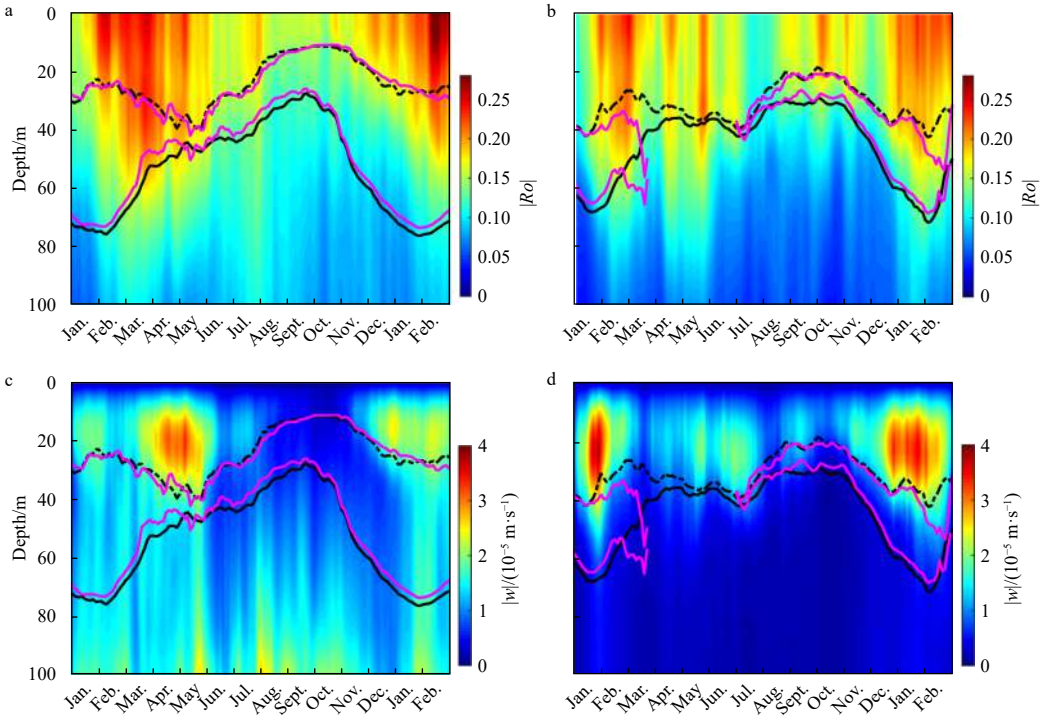

Fig. 13. Temporal evolution of $|Ro|$ (a) and $|w|$ (c) averaged over the northern region. b and d are the same as a and c, but for the central region. The dashed and solid black lines denote mixed layer depth (MLD) and isothermal layer depth (ILD), respectively. The layer between the magenta lines is the temperature inversion layer (TIL).

though submesoscale motions are mainly confined in the upper mixed layer, high values of *Ro* also appear under the mixed layer (Figs 13a, b). During the summer monsoon, submesoscale motions are relatively weaker and concentrate within the mixed layer in both NR and CR. However, in the winter and spring, they can penetrate far beneath the base of the mixed layer and into the BL, even into the thermocline layer. For example, the active submesoscale motions extend to 65 m in March in NR, when the MLD is only 30 m. In CR, high *Ro* signals reach 50 m, which exceeds the MLD of approximately 30 m in February. Strong submesoscale motions can even reach beneath the isothermal layer, such as over NR and CR in May. The vertical motions obviously strengthen when the mixed layer is deeper (Figs 13c, d). The deeper MLD seems to provide a favorable condition for horizontally tilting of outcropping isopycnals and subsequently inducing strong vertical exchange.

The depth-time evolution of N^2, N_S^2, and N_T^2 averaged over NR and CR is shown in Fig. 14. As expected, the BL and TIL are high stratification layers (Figs 14a, b). The upper stratification is dominated by salinity rather than temperature (Figs 14c, d). The blue contours in Fig. 14 are the regionally-averaged *Ro* of 0.18. The 0.18 of *Ro* represents the discrimination between the strong and weak submesoscale motions.

The vertical distribution of the submesoscale motions seems to correlate with MLD and the stratification below it. Deep MLD favors active submesoscale motions generating, and strong stratification inhibits the deepen of the active submesoscale motion. In NR (Fig. 14a), when the MLD is shallowest and the stratification is strongest (August–October), submesoscale motions are the weakest and strictly trapped in the shallow mixed layer. During the late fall, the strong salinity stratification goes deeper and becomes thicker, but the presence of temperature inversion partially counteracts the salinity stratification (Fig. 14e). Submesoscale motions are mostly restricted in the mixed layer due to the still relatively strong stratification below it. When comes to winter, deep mixed layer and thick BL present. Constrain by the stratification in the thick BL, the strong submesoscale motions only extend to the interior of the BL and TIL. Differently, in the spring, the ILD begins to shoal and the stratified layer turns weak and thin, which is probably due to surface heating and the vertical mixing (Thadathil et al., 2007). Without the constraint, strong submesoscale signals penetrate to larger depths and even pass through the BL.

Similarly, the high *Ro* processes in CR have a corresponding relationship to the vertical stratification. The columns of high submesoscale motions are potentially limited by the stratification contained in the BL and TIL during the winter monsoon. The maximum extended depth is at the interior of the BL. When the

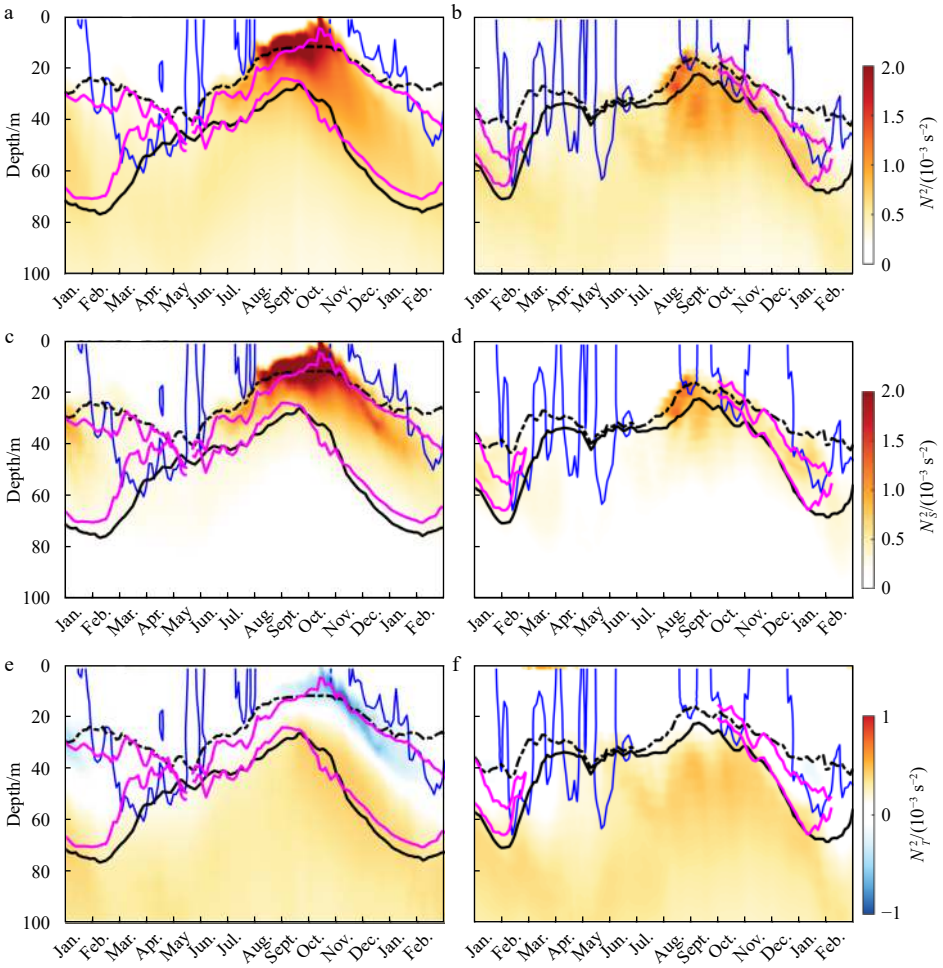

Fig. 14. Temporal and depth evolution of the density stratification (color) N^2 (a, b), and the component of salinity N_S^2(c, d), temperature $N_T{}^2$ (e, f) in northern region (left) and central region (right). The blue contours are the *Ro* that is 0.18. The black and magenta lines are the same in Fig. 13.

BL is thinner and has weak stratification in spring, the depth of strong submesoscale motions even stretches into the thermocline. When compared with NR, the BL is thinner and the stratification is weaker in CR, and the active submesoscale processes can extend to further distance below the mixed layer.

6 Conclusions and discussion

Based on high resolution numerical simulation data from ROMS, the features of submesoscale motions in the northern BoB are characterized in this article. Compared with the HR results, submesoscale motions in LR are much weaker. The northern BoB experiences obvious seasonality in terms of the dynamical characteristics of submesoscale motions, with stronger signals in the winter and spring but weaker in the summer and fall. Diagnostic analysis reveals the occurrence of submesoscale motions mainly trapped in the mixed layer, but they can penetrate under the base of the mixed layer. The MLIs appear to play a more important role than frontogenesis in the formation of the submesoscale in this region. The conspicuous seasonality of submesoscale motions is tightly associated with the variations in MLD, which are probably modulated by the influxes of freshwater as well as large and mesoscale motions. Further analysis implies that the mixed layer and the stratification below affect the vertical distribution of submesoscale motions. When the vertical salinity gradients over the BL are weakest, high *Ro* motions can reach depths far beyond the BL. However, the thick and high stratification BL seems to act as a buffer in which the depth of submesoscale motions is limited.

In this study, we qualitatively study the relationship of the two generating mechanisms and submesoscale motions, respectively. Actually, frontogenesis and MLIs cannot separate from each other, they are tightly related (McWilliams, 2016). The pre-exist weak fronts are sharply intensified by frontogenesis, and accompanied by the MLIs. Our findings display the potential influence of frontogenesis and MLIs on submesoscale motions. Besides, symmetry instability, buoyancy forcing, topography and tides are contributing to the formation of submesoscale motions. Submesoscale characteristics and the mechanisms need further explored with more dedicated numerical simulation outputs with finer spatial resolution and higher frequency temporal interval.

Acknowledgements

The RAMA buoy data was obtained from https://www.pmel.noaa.gov/gtmba/pmel-theme/indian-ocean-rama. The sea surface height data is distributed at AVISO and can be downloaded from http://marine.copernicus.eu/. The high-resolution SST from MODIS is available at https://oceancolor.gsfc.nasa.gov/. The reconstructed Argo products were obtained from http://www.umr-lops.fr/. The QuikSCAT wind stress data is available at http://www.ifremer.fr/opendap/cerdap1/cersat/wind/l4/quikscat/daily/. The freshwater and hear flux data were produced by the Asia-Pacific Data-Research Center (http://apdrc.soest.hawaii.edu/dods/public_data/iCOADS/). The SODA reanalysis dataset was provided by http://apdrc.soest.hawaii.edu/dods/public_data/SODA/. The GEBCO topography dataset was produced by the British Oceanographic Date Centre (http://data.nodc.noaa.gov/).

References

Akhil V P, Durand F, Lengaigne M, et al. 2014. A modeling study of the processes of surface salinity seasonal cycle in the Bay of Bengal. Journal of Geophysical Research: Oceans, 119(6): 3926–3947, doi: 10.1002/2013JC009632

Babu M T, Kumar P S, Rao D P. 1991. A subsurface cyclonic eddy in the Bay of Bengal. Journal of Marine Research, 49(3): 403–410, doi: 10.1357/002224091784995846

Balaguru K, Chang Ping, Saravanan R, et al. 2012. Ocean barrier layers' effect on tropical cyclone intensification. Proceedings of the National Academy of Sciences of the United States of America, 109(36): 14343–14347, doi: 10.1073/pnas.1201364109

Behara A, Vinayachandran P N. 2016. An OGCM study of the impact of rain and river water forcing on the Bay of Bengal. Journal of Geophysical Research: Oceans, 121(4): 2425–2446, doi: 10.1002/2015JC011325

Boccaletti G, Ferrari R, Fox-Kemper B. 2007. Mixed layer instabilities and restratification. Journal of Physical Oceanography, 37(9): 2228–2250, doi: 10.1175/JPO3101.1

Brannigan L, Marshall D P, Naveira-Garabato A, et al. 2015. The seasonal cycle of submesoscale flows. Ocean Modelling, 92: 69–84, doi: 10.1016/j.ocemod.2015.05.002

Buckingham C E, Garabato A C N, Thompson A F, et al. 2016. Seasonality of submesoscale flows in the ocean surface boundary layer. Geophysical Research Letters, 43(5): 2118–2126, doi: 10.1002/2016GL068009

Callies J, Ferrari R, Klymak J M, et al. 2015. Seasonality in submesoscale turbulence. Nature Communications, 6(1): 6862, doi: 10.1038/ncomms7862

Cao Haijin, Fox-Kemper B, Jing Zhiyou. 2021. Submesoscale eddies in the upper ocean of the kuroshio extension from high-resolution simulation: energy budget. Journal of Physical Oceanography, 51(7): 2181–2201, doi: 10.1175/JPO-D-20-0267.1

Capet X, Campos E J, Paiva A M. 2008a. Submesoscale activity over the Argentinian shelf. Geophysical Research Letters, 35(15): L15605, doi: 10.1029/2008GL034736

Capet X, McWilliams J C, Molemaker M J, et al. 2008b. Mesoscale to submesoscale transition in the California Current system. Part I: flow structure, eddy flux, and observational tests. Journal of Physical Oceanography, 38(1): 29–43, doi: 10.1175/2007JPO3671.1

Capet X, McWilliams J C, Molemaker M J, et al. 2008c. Mesoscale to submesoscale transition in the California Current system. Part II: frontal processes. Journal of Physical Oceanography, 38(1): 44–64, doi: 10.1175/2007JPO3672.1

Capet X, McWilliams J C, Molemaker M J, et al. 2008d. Mesoscale to submesoscale transition in the California Current system. Part III: energy balance and flux. Journal of Physical Oceanography, 38(10): 2256–2269, doi: 10.1175/2008JPO3810.1

Carton J A, Giese B S. 2008. A reanalysis of ocean climate using Simple Ocean Data Assimilation (SODA). Monthly Weather Review, 136(8): 2999–3017, doi: 10.1175/2007MWR1978.1

Chen Gengxin, Wang Dongxiao, Hou Yijun. 2012. The features and interannual variability mechanism of mesoscale eddies in the Bay of Bengal. Continental Shelf Research, 47: 178–185, doi: 10.1016/j.csr.2012.07.011

Cheng Xuhua, McCreary J P, Qiu Bo, et al. 2018. Dynamics of eddy generation in the central Bay of Bengal. Journal of Geophysical Research: Oceans, 123(9): 6861–6875, doi: 10.1029/2018JC014100

Cheng Xuhua, Xie Shangping, McCreary J P, et al. 2013. Intraseasonal variability of sea surface height in the Bay of Bengal. Journal of Geophysical Research: Oceans, 118(2): 816–830, doi: 10.1002/jgrc.20075

Dandapat S, Gnanaseelan C, Parekh A. 2020. Impact of excess and deficit river runoff on Bay of Bengal upper ocean characteristics using an ocean general circulation model. Deep-Sea Research Part II: Topical Studies in Oceanography, 172: 104714, doi: 10.1016/j.dsr2.2019.104714

Dong Jihai, Fox-Kemper B, Zhang Hong, et al. 2020. The seasonality of submesoscale energy production, content, and cascade. Geophysical Research Letters, 47(6): e2020GL087388, doi: 10.1029/2020GL087388

Dong Jihai, Zhong Yisen. 2018. The spatiotemporal features of submesoscale processes in the northeastern South China Sea. Acta Oceanologica Sinica, 37(11): 8–18, doi: 10.1007/s13131-018-1277-2

Eigenheer A, Quadfasel D. 2000. Seasonal variability of the Bay of Bengal circulation inferred from TOPEX/Poseidon altimetry. Journal of Geophysical Research: Oceans, 105(C2): 3243–3252, doi: 10.1029/1999JC900291

Fox-Kemper B, Ferrari R. 2008. Parameterization of mixed layer eddies. Part II: prognosis and impact. Journal of Physical Oceanography, 38(6): 1166–1179, doi: 10.1175/2007JPO3788.1

Fox-Kemper B, Ferrari R, Hallberg R. 2008. Parameterization of mixed layer eddies. Part I: theory and diagnosis. Journal of Physical Oceanography, 38(6): 1145–1165, doi: 10.1175/2007JPO3792.1

Girishkumar M S, Ravichandran M, McPhaden M J. 2013. Temperature inversions and their influence on the mixed layer heat budget during the winters of 2006–2007 and 2007–2008 in the Bay of Bengal. Journal of Geophysical Research: Oceans, 118(5): 2426–2437, doi: 10.1002/jgrc.20192

Gula J, Molemaker M J, McWilliams J C. 2014. Submesoscale cold filaments in the Gulf Stream. Journal of Physical Oceanography, 44(10): 2617–2643, doi: 10.1175/JPO-D-14-0029.1

Han Weiqing, Lawrence D M, Webster P J. 2001. Dynamical response of equatorial Indian Ocean to intraseasonal winds: zonal flow. Geophysical Research Letters, 28(22): 4215–4218, doi: 10.1029/2001GL013701

Hoskins B J. 1982. The mathematical theory of frontogenesis. Annual Review of Fluid Mechanics, 14: 131–151, doi: 10.1146/annurev.fl.14.010182.001023

Hoskins B J, Bretherton F P. 1972. Atmospheric frontogenesis models: mathematical formulation and solution. Journal of the Atmospheric Sciences, 29(1): 11–37, doi: 10.1175/1520-0469(1972)029<0011:AFMMFA>2.0.CO;2

Howden S D, Murtugudde R. 2001. Effects of river inputs into the Bay of Bengal. Journal of Geophysical Research: Oceans, 106(C9): 19825–19843, doi: 10.1029/2000JC000656

Jing Zhiyou, Fox-Kemper B, Cao Haijin, et al. 2021. Submesoscale fronts and their dynamical processes associated with symmetric instability in the Northwest Pacific subtropical ocean. Journal of Physical Oceanography, 51(1): 83–100, doi: 10.1175/JPO-D-20-0076.1

Jithin A K, Subeesh M P, Francis P A, et al. 2020. Intensification of tidally generated internal waves in the north-central Bay of Bengal. Scientific Reports, 10(1): 6059, doi: 10.1038/s41598-020-62679-4

Klein P, Lapeyre G. 2009. The oceanic vertical pump induced by mesoscale and submesoscale turbulence. Annual Review of Marine Science, 1: 351–375, doi: 10.1146/annurev.marine.010908.163704

Large W G, McWilliams J C, Doney S C. 1994. Oceanic vertical mixing: a review and a model with a nonlocal boundary layer parameterization. Reviews of Geophysics, 32(4): 363–403, doi: 10.1029/94RG01872

Lévy M, Resplandy L, Klein P, et al. 2012. Grid degradation of submesoscale resolving ocean models: Benefits for offline passive tracer transport. Ocean Modelling, 48: 1–9, doi: 10.1016/j.ocemod.2012.02.004

Lin Hongyang, Liu Zhiyu, Hu Jianyu, et al. 2020. Characterizing meso- to submesoscale features in the South China Sea. Progress in Oceanography, 188: 102420, doi: 10.1016/j.pocean.2020.102420

Luo Hao, Bracco A, Cardona Y, et al. 2016. Submesoscale circulation in the northern Gulf of Mexico: surface processes and the impact of the freshwater river input. Ocean Modelling, 101: 68–82, doi: 10.1016/j.ocemod.2016.03.003

Ma Tian, Cheng Xuhua, Qi Yiquan, et al. 2020. Interannual variability in the barrier layer and forcing mechanism in the eastern equatorial Indian Ocean and Bay of Bengal. Acta Oceanologica Sinica, 39(7): 19–31, doi: 10.1007/s13131-020-1575-3

Maes C. 2008. On the ocean salinity stratification observed at the eastern edge of the equatorial Pacific Warm Pool. Journal of Geophysical Research: Oceans, 113(C3): C03027, doi: 10.1029/2007JC004297

Mahadevan A. 2016. The impact of submesoscale physics on primary productivity of plankton. Annual Review of Marine Science, 8: 161–184, doi: 10.1146/annurev-marine-010814-015912

Mahadevan A, Tandon A. 2006. An analysis of mechanisms for submesoscale vertical motion at ocean fronts. Ocean Modelling, 14(3–4): 241–256, doi: 10.1016/j.ocemod.2006.05.006

McWilliams J C. 2016. Submesoscale currents in the ocean. Proceedings of the Royal Society A: Mathematical, Physical and Engineering Sciences, 472(2189): 20160117, doi: 10.1098/rspa.2016.0117

McWilliams J C. 2017. Submesoscale surface fronts and filaments: secondary circulation, buoyancy flux, and frontogenesis. Journal of Fluid Mechanics, 823: 391–432, doi: 10.1017/jfm.2017.294

Mensa J A, Garraffo Z, Griffa A, et al. 2013. Seasonality of the submesoscale dynamics in the Gulf Stream region. Ocean Dynamics, 63(8): 923–941, doi: 10.1007/s10236-013-0633-1

Molemaker M J, McWilliams J C, Capet X. 2010. Balanced and unbalanced routes to dissipation in an equilibrated Eady flow. Journal of Fluid Mechanics, 654: 35–63, doi: 10.1017/S0022112009993272

Molemaker M J, McWilliams J C, Dewar W K. 2015. Submesoscale instability and generation of mesoscale anticyclones near a separation of the California undercurrent. Journal of Physical Oceanography, 45(3): 613–629, doi: 10.1175/JPO-D-13-0225.1

Narvekar J, Kumar S P. 2006. Seasonal variability of the mixed layer in the central Bay of Bengal and associated changes in nutrients and chlorophyll. Deep-Sea Research Part I: Oceanographic Research Papers, 53(5): 820–835, doi: 10.1016/j.dsr.2006.01.012

Neetu S, Lengaigne M, Vincent E M, et al. 2012. Influence of upper-ocean stratification on tropical cyclone-induced surface cooling in the Bay of Bengal. Journal of Geophysical Research: Oceans, 117(C12): C12020, doi: 10.1029/2012JC008433

Pham H T, Sarkar S. 2019. The role of turbulence in strong submesoscale fronts of the Bay of Bengal. Deep-Sea Research Part II: Topical Studies in Oceanography, 168: 104644, doi: 10.1016/j.dsr2.2019.104644

Phaniharam S A, Chintam V, Baggu G, et al. 2020. Study of internal wave characteristics off northwest Bay of Bengal using synthetic aperture radar. Natural Hazards, 104(3): 2451–2460, doi: 10.1007/s11069-020-04280-6

Qiu Yun, Cai Wenju, Li Li, et al. 2012. Argo profiles variability of barrier layer in the tropical Indian Ocean and its relationship with the Indian Ocean Dipole. Geophysical Research Letters, 39(8): L08605, doi: 10.1029/2012GL051441

Qiu Bo, Chen Shuiming, Klein P, et al. 2014. Seasonal mesoscale and submesoscale eddy variability along the North Pacific Subtropical Countercurrent. Journal of Physical Oceanography, 44(12): 3079–3098, doi: 10.1175/JPO-D-14-0071.1

Qiu Yun, Li Li, Yu Weidong, et al. 2007. Annual and interannual variations of sea-level anomaly in the Bay of Bengal and the Andaman Sea. Acta Oceanologica Sinica, 26(6): 13–29

Rahaman H, Ravichandran M, Sengupta D, et al. 2014. Development of a regional model for the North Indian Ocean. Ocean Modelling, 75: 1–19, doi: 10.1016/j.ocemod.2013.12.005

Ramachandran S, Tandon A. 2020. Generation of submesoscale temperature inversions below salinity fronts in the Bay of Bengal. Journal of Geophysical Research: Oceans, 125(12): e2020JC016278, doi: 10.1029/2020JC016278

Ramachandran S, Tandon A, Mackinnon J, et al. 2018. Submesoscale processes at shallow salinity fronts in the Bay of Bengal: observations during the winter monsoon. Journal of Physical Oceanography, 48(3): 479–509, doi: 10.1175/JPO-D-16-0283.1

Rao R R, Sivakumar R. 2003. Seasonal variability of sea surface salinity and salt budget of the mixed layer of the North Indian Ocean. Journal of Geophysical Research, 108(C1): 3009, doi: 10.1029/2001JC000907

Sarkar S, Pham H T, Ramachandran S, et al. 2016. The interplay between submesoscale instabilities and turbulence in the surface layer of the Bay of Bengal. Oceanography, 29(2): 146–157, doi: 10.5670/oceanog.2016.47

Schott F A, Xie Shangping, McCreary J P Jr. 2009. Indian Ocean circulation and climate variability. Reviews of Geophysics, 47(1): RG1002, doi: 10.1029/2007RG000245

Sengupta D, Goddalehundi B R, Anitha D S. 2008. Cyclone-induced mixing does not cool SST in the post-monsoon north Bay of Bengal. Atmospheric Science Letters, 9(1): 1–6, doi: 10.1002/asl.162

Sengupta D, Raj G N B, Ravichandran M, et al. 2016. Near-surface salinity and stratification in the north Bay of Bengal from moored observations. Geophysical Research Letters, 43(9): 4448–4456, doi: 10.1002/2016GL068339

Shchepetkin A F, McWilliams J C. 2005. The regional oceanic modeling system (ROMS): a split-explicit, free-surface, topography-following-coordinate oceanic model. Ocean Modelling, 9(4): 347–404, doi: 10.1016/j.ocemod.2004.08.002

Shetye S R. 1993. The movement and implications of the Ganges-Brahmaputra runoff on entering the Bay of Bengal. Current Science, 64(1): 32–38

Somayajulu Y K, Murty V S N, Sarma Y V B. 2003. Seasonal and inter-annual variability of surface circulation in the Bay of Bengal from TOPEX/Poseidon altimetry. Deep-Sea Research Part II: Topical Studies in Oceanography, 50(5): 867–880, doi: 10.1016/S0967-0645(02)00610-0

Su Zhan, Wang Jinbo, Klein P, et al. 2018. Ocean submesoscales as a key component of the global heat budget. Nature Communications, 9(1): 775, doi: 10.1038/s41467-018-02983-w

Suresh I, Vialard J, Lengaigne M, et al. 2013. Origins of wind-driven intraseasonal sea level variations in the North Indian Ocean coastal waveguide. Geophysical Research Letters, 40(21): 5740–5744, doi: 10.1002/2013GL058312

Tazkia A R, Krien Y, Durand F, et al. 2017. Seasonal modulation of M_2 tide in the northern Bay of Bengal. Continental Shelf Research, 137: 154–162, doi: 10.1016/j.csr.2016.12.008

Thadathil P, Muraleedharan P M, Rao R R, et al. 2007. Observed seasonal variability of barrier layer in the Bay of Bengal. Journal of Geophysical Research: Oceans, 112(C2): C02009, doi: 10.1029/2006JC003651

Thadathil P, Suresh I, Gautham S, et al. 2016. Surface layer temperature inversion in the Bay of Bengal: main characteristics and related mechanisms. Journal of Geophysical Research: Oceans, 121(8): 5682–5696, doi: 10.1002/2016JC011674

Thomas L N, Tandon A, Mahadevan A. 2008. Submesoscale processes and dynamics. Ocean Modeling in an Eddying Regime, 177: 17–38, doi: 10.1029/177GM04

Torres H S, Klein P, Menemenlis D, et al. 2018. Partitioning ocean motions into balanced motions and internal gravity waves: a modeling study in anticipation of future space missions. Journal of Geophysical Research: Oceans, 123(11): 8084–8105, doi: 10.1029/2018JC014438

Vialard J, Shenoi S S C, McCreary J P, et al. 2009. Intraseasonal response of the northern Indian Ocean coastal waveguide to the Madden-Julian Oscillation. Geophysical Research Letters, 36(14): L14606, doi: 10.1029/2009GL038450

Vinayachandran P N, Murty V S N, Babu V R. 2002. Observations of barrier layer formation in the Bay of Bengal during summer monsoon. Journal of Geophysical Research: Oceans, 107(C12): 8018, doi: 10.1029/2001JC000831

Wang Shengpeng, Jing Zhao, Liu Hailong, et al. 2018. Spatial and seasonal variations of submesoscale eddies in the eastern tropical Pacific Ocean. Journal of Physical Oceanography, 48(1): 101–116, doi: 10.1175/JPO-D-17-0070.1

Woodruff S D, Worley S J, Lubker S J, et al. 2011. ICOADS Release 2.5: extensions and enhancements to the surface marine meteorological archive. International Journal of Climatology, 31(7): 951–967, doi: 10.1002/joc.2103

Yang Qingxuan, Zhao Wei, Liang Xinfeng, et al. 2017. Elevated mixing in the periphery of mesoscale eddies in the South China Sea. Journal of Physical Oceanography, 47(4): 895–907, doi: 10.1175/JPO-D-16-0256.1

Zhang Zhiwei, Zhang Yuchen, Qiu Bo, et al. 2020. Spatiotemporal characteristics and generation mechanisms of submesoscale currents in the northeastern South China Sea revealed by numerical simulations. Journal of Geophysical Research: Oceans, 125(2): e2019JC015404, doi: 10.1029/2019JC015404

Supplementary information:

Fig. S1. The ratio of DIV and RV contribution to KE spectrum varies with wave number. The black contours represent the ratio equal to 0.1. The gray line represents the average wavelength corresponding to 0.1 isocline over the entire period.

Fig. S2. The snapshot of density at surface in April 29 (a), and December 29 (b).

The supplementary information is available online at https://10.1007/s13131-021-1847-6 and www.aosocean.com. The supplementary information is published as submitted, without typesetting or editing. The responsibility for scientific accuracy and content remains entirely with the authors.